Meissner-like effect for synthetic gauge field in multimode cavity QED

Kyle E. Ballantine,[1] Benjamin L. Lev,[2] and Jonathan Keeling[1]

[1] *SUPA, School of Physics and Astronomy, University of St. Andrews, St. Andrews KY16 9SS, United Kingdom*
[2] *Departments of Physics and Applied Physics and Ginzton Laboratory, Stanford University, Stanford CA 94305, USA*

Previous realizations of synthetic gauge fields for ultracold atoms do not allow the spatial profile of the field to evolve freely. We propose a scheme which overcomes this restriction by using the light in a multimode cavity with many nearly degenerate transverse modes, in conjunction with Raman coupling, to realize an artificial magnetic field which acts on a Bose-Einstein condensate of neutral atoms. We describe the evolution of such a system, and present the results of numerical simulations which show dynamical coupling between the effective field and the matter on which it acts. Crucially, the freedom of the spatial profile of the field is sufficient to realize a close analogue of the Meissner effect, where the magnetic field is expelled from the superfluid. This back-action of the atoms on the synthetic field distinguishes the Meissner-like effect described here from the Hess-Fairbank suppression of rotation in a neutral superfluid observed elsewhere.

The Meissner effect [1] is the *sine qua non* of superconductivity [2]. As captured by the Ginzburg-Landau equations [3], the superfluid order parameter couples to the electromagnetic fields such that there is perfect diamagnetism. Physically this arises because the normal paramagnetic response of matter is completely suppressed by the phase stiffness of the superfluid, leaving only the diamagnetic current [4]. Magnetic field thus decays exponentially into the bulk [5]. Exponentially decaying fields are symptomatic of a massive field theory, and so can be seen as a direct consequence of the the Anderson-Higgs mechanism [6, 7] giving the electromagnetic field a mass gap. Central to all these phenomena is that minimal coupling between the electromagnetic field and the superfluid modifies the equations of motion for both the superfluid and the electromagnetic field.

The concept of "synthetic" gauge fields has attracted much attention over the last few years. In the context of ultracold atoms, realizations have included schemes based on dark states [8, 9] or Raman driving [10–12], or inducing Peierls phases in lattice systems [13–23] (for a review, see [24–27]). There have also been proposals to realize gauge fields for photons, including "free space" realizations using Rydberg atoms in non-planar ring cavity geometries [28] as well as Peierls phases for photon hopping in coupled cavity arrays [29–31]. However, with a few exceptions, all these have involved static gauge fields—there is no feedback of the atoms (or photons) on the synthetic field. Thus, even in the pioneering demonstration of a Meissner phase of chiral currents [23], it is noted that these experiments are closer to the Hess-Fairbank effect [32] (suppression of rotation in a neutral superfluid), and do not show expulsion of the synthetic field. In contrast, a charged superfluid acts back on the magnetic field.

The synthetic field cannot be expelled in the above schemes because it is set by a fixed external laser or the system geometry. The exceptions are thus proposals where the strength of synthetic field depends on a dynamical quantity. One such proposal is in optomechanical cavity arrays with a Peierls phase for photon hopping set by mechanical oscillators [33]. Another proposal is to consider atoms in optical cavities, replacing the external laser drive by light in the cavity, as has been recently proposed by Zheng and Cooper [34], with a two photon-assisted hopping scheme involving the cavity and a transverse pump. This scheme naturally relates to the self-organization of atoms under transverse pumping [35–37], and proposed extensions involving spin-orbit coupling [38–42] and self-organized chiral states [43, 44]. However, in these schemes, a single-mode cavity is used, giving a "mean-field" coupling due to the infinite-range nature of the interactions, and not the local coupling to the gauge potential present in the Ginzburg-Landau equations.

Locality can be restored in a multimode cavity—in a cavity that supports multiple nearly degenerate transverse modes one can build localized wavepackets [45]. This is also illustrated for a longitudinally pumped system when considering the Talbot effect [46] with cold atoms [47]: When atoms are placed in front of a planar mirror and illuminated with coherent light, phase modulation of the light is transformed by propagation into intensity modulation, leading to self-organization. This effect can be viewed as an effective atom-atom interaction mediated by light, leading to density-wave formation [48–50]. In this Letter, we show how multimode cavity QED [45, 51–54] can be used to realize a dynamical gauge field for cold atoms capable of realizing an analogue of the Meissner effect for charged superfluids. The simultaneous presence of near-degenerate cavity modes allows the spatial intensity profile of the cavity light field to change over time in response to the state of the atoms, in a form directly analogous to the Ginzburg-Landau equations.

By realizing such a multimode cavity QED simulator of matter and dynamical gauge fields, numerous possibilities arise. Most intriguingly, the tunability of the parameters controlling the effective matter-light coupling potentially allow one to simulate the behavior of mat-

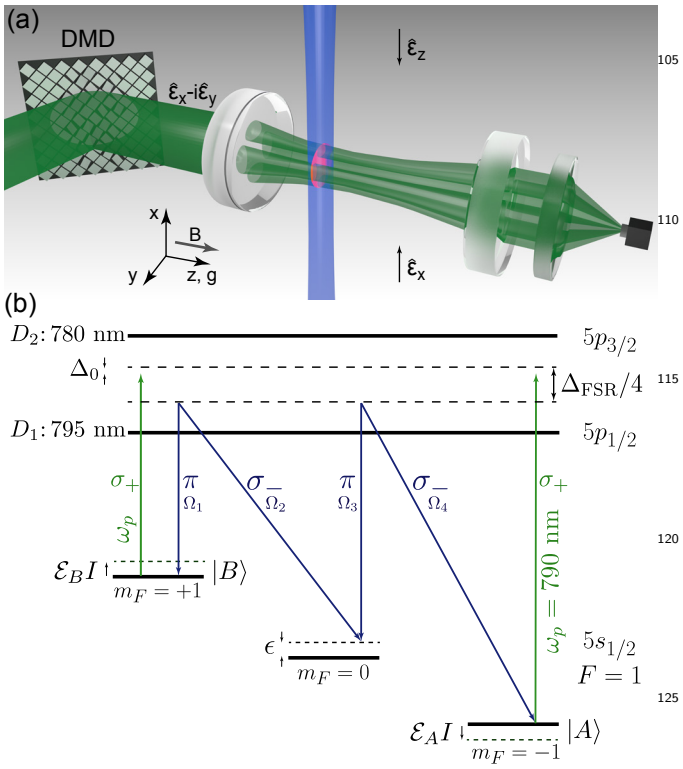

FIG. 1. (a) A 2D-BEC is coupled to linearly polarized counter-propagating Raman beams in $\hat{x}$ and trapped inside a cavity set in the multimode, confocal configuration. (Optical trapping lasers not shown, and only TEM_{10} and TEM_{01} modes shown for simplicity.) The axis of the oblate BEC is collinear with the cavity axis. The cavity, with field loss κ, is pumped along $+\hat{z}$ by a circularly polarized field of frequency ω_p detuned by Δ_0 from the confocal cavity frequency ω_0. The pump laser is spatially shaped with a digital multimirror device (DMD) spatial light modulator before cavity injection. Cavity light is imaged by an EMCCD camera. (Atomic absorption imaging laser and camera not shown.) A magnetic field B is oriented along $+\hat{z}$. (b) ^{87}Rb atomic level diagram with three coupling lasers shown. Green arrows show the pump field that Stark shifts the state $|A\rangle$ and $|B\rangle$ by $\mathcal{E}_{A,B}$. The laser frequency is set to the tune-out wavelength between the D_1 and D_2 lines in ^{87}Rb. The blue arrows show the two-photon Raman-coupling fields driving π and σ_- transitions—effected by obeying electric dipole selection rules for the polarizations given in panel (a)—with Rabi frequencies Ω_i. The Raman fields are detuned from ω_0 by a quarter of a free spectral range $\Delta_{FSR}/4$ and the $m = 0$ state is detuned by ϵ via the quadratic Zeeman shift.

ter with alternate values of the fine structure constant α. This could provide a continuum gauge field theory simulator complementary to the proposals for simulating lattice gauge field theories using ultracold atoms [55–65], trapped ions [66–69], or superconducting circuits [70, 71]. Other opportunities arising from our work are to explore the differences between Bose-condensed, thermal, and fermionic atoms in the geometry considered above: The Meissner effect depends on the phase stiffness of superfluid atoms, so should vanish at higher temperatures. For fermions, one might use synthetic field expulsion as a probe of BCS superfluidity.

Our proposal is based on the confocal cavity system recently realized by Kollár *et al.* [53, 54]. This cavity may be tuned between confocal multimode and single-mode configurations. In addition, light can be pumped transversely or longitudinally, and patterned using a digital light modulator [72]. Multimode cavity QED has previously been proposed to explore beyond mean-field physics in the self-organization of ultracold atoms [45, 51, 54].

We consider this cavity in the near-confocal case, so that many modes are near-degenerate. This cavity contains a 2D-condensate of atoms confined along the cavity axis as shown in Fig. 1. These atoms have two low-lying internal states, $|A\rangle$ and $|B\rangle$, which are coupled by two counter-propagating Raman beams via a higher intermediate state, for example, considering bosonic ^{87}Rb, one may create an effective two-level system from three $F = 1$ levels by noting that the $m = \pm 1$ levels, split by a magnetic field [10, 12], can be coupled via the $m = 0$ state, which can be off-resonant due to the quadratic Zeeman shift ϵ, as previously shown in Refs. [12, 73]. If the population of the excited state is negligible, the Raman beams lead to an effective Rabi coupling $\Omega \propto (\prod_{i=1}^{4} \Omega_i)/\Delta_A^2 \epsilon$ between the two lower states, which in the scheme suggested in Fig. 1 is fourth order and where Δ_A is the effective detuning from the excited states. An atom in state $|A\rangle$ gains momentum $q\hat{x}$ by absorbing two photons from one transverse beam, and loses momentum $-q\hat{x}$ by emitting two photons into the other beam, finishing in state $|B\rangle$, where $q/2 = 2\pi/\lambda$ is the momentum of the Raman beams. Hence, the two states have momentum differing by $2q\hat{x}$. Crucially, each state has a different Stark shift due to the interaction with many cavity photons contributing to the intensity I, with coefficients $\mathcal{E}_{A,B}$. This gives an atomic Hamiltonian of the form: $\hat{H}_{\rm atom} = \int d^2\mathbf{r}\, \mathrm{d}z \tilde{\Psi}^\dagger_{\mathbf{r},z}[\mathbf{h} + V_{\rm ext}(\mathbf{r}, z)]\tilde{\Psi}_{\mathbf{r},z} + \hat{H}_{\rm int}$, where

$$\mathbf{h} = \begin{pmatrix} \frac{(-i\nabla - q\hat{\mathbf{x}})^2}{2m} - \mathcal{E}_A I(\mathbf{r},z) & \Omega/2 \\ \Omega/2 & \frac{(-i\nabla + q\hat{\mathbf{x}})^2}{2m} - \mathcal{E}_B I(\mathbf{r},z) \end{pmatrix}. \quad (1)$$

For simplicity, here and in the following, we write $\mathbf{r} = (x, y)$, with the z-dependence written separately, and set $\hbar = 1$. The term $\hat{H}_{\rm int}$ describes contact interactions between atoms with strength U.

The cavity pump field wavelength is set to be at the "tune-out" point, 790.018 nm, between the D_1 and D_2 lines in ^{87}Rb [74]. The scalar light shift is zero at this wavelength, which means that the atom trapping frequencies are nearly unaffected by the cavity light in the absence of Raman coupling. The vector light shift is approximately equal and opposite for states $|A\rangle$ and $|B\rangle$ due to their opposite m_F projections, i.e., $\mathcal{E}_A = -\mathcal{E}_B$. Spontaneous emission is low, less than $\sim$10 Hz for the required Stark shifts, since this light is far detuned from

either excited state. The Raman coupling scheme is identical to those in Refs. [12, 73] that exhibited nearly 0.5-s spontaneous-emission-limited BEC lifetimes. The Raman lasers do not scatter into the cavity, since they are detuned $\Delta_{\rm FSR}/4 = 3.25$ GHz from any family of degenerate cavity modes for a $L = 1$-cm confocal cavity [53]. The BEC lifetime under our cavity and Raman-field dressing scheme should therefore be more than 100 ms, sufficient to observe the predicted physics.

The artificial magnetic field that arises from the Raman driving scheme is in $\hat{z}$ [10], and so the interesting atomic dynamics will be in the transverse ($\hat{x}$-$\hat{y}$) plane. We therefore consider a 2D pancake of atoms, with strong trapping in $\hat{z}$, such that we may write $\Psi_{A,B}(\mathbf{r}, z) = \psi_{A,B}(\mathbf{r})Z(z)$, where $Z(z)$ is a narrow Gaussian profile due to the strong trapping in $\hat{z}$. In this strong trapping limit, we can integrate out the z dependence to produce effective equations of motion for the transverse wavefunctions $\psi_{A,B}$ and the transverse part of the cavity light field φ. We consider the case where the atom cloud is trapped near one end of the cavity, $z_0 \simeq \pm z_R$, as this leads to a quasi-local coupling between atoms and cavity light (see supplemental material [75] for details). We choose to normalize the atomic wavefunctions such that $\int \mathrm{d}^2\mathbf{r}\ \left(|\psi_A|^2 + |\psi_B|^2\right) = 1$ so that the number of atoms N appears explicitly. The transverse equations of motion then take the form:

$$i\partial_t\varphi = \left[\frac{\delta}{2}\left(-l^2\nabla^2 + \frac{r^2}{l^2}\right) - \Delta_0 - i\kappa - N\mathcal{E}_\Sigma\left(|\psi_A|^2 + |\psi_B|^2\right) - N\mathcal{E}_\Delta(|\psi_A|^2 - |\psi_B|^2)\right]\varphi + f(\mathbf{r}), \tag{2}$$

$$i\partial_t\begin{pmatrix}\psi_A\\ \psi_B\end{pmatrix} = \left[-\frac{\nabla^2}{2m} + V_{\rm ext}(\mathbf{r}) - \mathcal{E}_\Sigma|\varphi|^2 + NU\left(|\psi_A|^2 + |\psi_B|^2\right) + \begin{pmatrix}-\mathcal{E}_\Delta|\varphi|^2 + i\frac{q}{m}\partial_x & \Omega/2\\ \Omega/2 & \mathcal{E}_\Delta|\varphi|^2 - i\frac{q}{m}\partial_x\end{pmatrix}\right]\begin{pmatrix}\psi_A\\ \psi_B\end{pmatrix}. \tag{3}$$

Here we have rewritten $\mathcal{E}_\Sigma = (\mathcal{E}_A + \mathcal{E}_B)/4$ and $\mathcal{E}_\Delta = (\mathcal{E}_A - \mathcal{E}_B)/4$. $\Delta_0 = \omega_P - \omega_0$ is the detuning of the pump from the confocal cavity frequency ω_0, and $f(\mathbf{r})$ is the pump profile. We are considering modes in a nearly confocal cavity for the cavity field φ [53]. In such a case, a given family of nearly degenerate modes takes the form of either even or odd Gauss-Hermite functions, where $\sqrt{2}l$ is the beam waist [76]. The first term in Eq. (2) is the real-space operator describing the splitting between the nearly degenerate modes when the cavity is detuned away from confocality with mode splitting δ. The restriction to only even modes means we must restrict to $\varphi(\mathbf{r}) = \varphi(-\mathbf{r})$; however, Eqs. (2) and (3) preserve this symmetry if it is initially present.

We first describe in general terms the behavior we can expect from Eqs. (2) and (3) before discussing the full steady-state of these equations. As this model is closely related to that proposed by Spielman [10], one may expect the same behavior to occur [12]. Namely, if we construct a basis transformation between the original levels and the dressed states $(\psi_+, \psi_-)^T = U(\psi_A, \psi_B)^T$ such that the atomic Hamiltonian is diagonalized, then atoms in each of these dressed states see effective (opposite) magnetic fields. The dispersion relation for the lower manifold (i.e., the non-interacting and translationally invariant part of the energy) has the form

$$E_-(\mathbf{k}) = \frac{1}{2m^*}\left(\mathbf{k} - Q|\varphi|^2\hat{\mathbf{x}}\right)^2 - \mathcal{E}_\Sigma|\varphi|^2 - \mathcal{E}_4|\varphi|^4 + \cdots, \tag{4}$$

which depends on the cavity light intensity $|\varphi|^2$. This can be recognized as the energy of a particle in a magnetic vector potential $\mathbf{A} = |\varphi|^2\hat{\mathbf{x}}$ with effective charge $Q = 2\mathcal{E}_\Delta q/(\Omega - 2q^2/m)$. The effective field experienced by the atoms is therefore proportional to the difference in the Stark shifts experienced by each level, as the average Stark shift simply leads to a scalar potential $\mathcal{E}_\Sigma|\phi|^2$. The atoms acquire an effective mass $m^* = m\Omega/(\Omega - 2q^2/m)$ because the eigenstate is in a superposition of states with differing momenta $k \pm q\hat{x}$. Finally, there is an additional scalar potential term proportional to $\mathcal{E}_4 = \mathcal{E}_\Delta^2/(\Omega - 2q^2/m)$, because each component experiences a different Stark shift. As $\Omega \to \infty$, the eigenstate approaches a symmetric superposition, the effective mass approaches m, and the extra scalar potential disappears.

As compared to Refs. [10, 12], the crucial difference in Eqs. (2) and (3) is that the atomic dynamics also acts back on the cavity light field φ. We can explore the nature of this back-action by expanding the low-energy eigenstate ψ_- to first order in $1/\Omega$. In the low-energy manifold, the difference $|\psi_A|^2 - |\psi_B|^2$ in Eq. (2) can be related to the wavefunction ψ_- by

$$|\psi_A|^2 - |\psi_B|^2 = \frac{q}{im\Omega}\left(\psi_-^*\partial_x\psi_- - \psi_-\partial_x\psi_-^*\right) + \frac{2\mathcal{E}_\Delta}{\Omega}|\psi_-|^2|\varphi|^2. \tag{5}$$

This has exactly the expected form of the effect of charged particles on a vector potential: there is a current dependent term, the first term, followed by a diamagnetic term. The current dependent term appearing in Eq. (2) would lead to a paramagnetic response. However in a superfluid state, this contribution is suppressed due to

the phase stiffness of the superfluid, and the surviving diamagnetic term then leads to the Meissner effect.

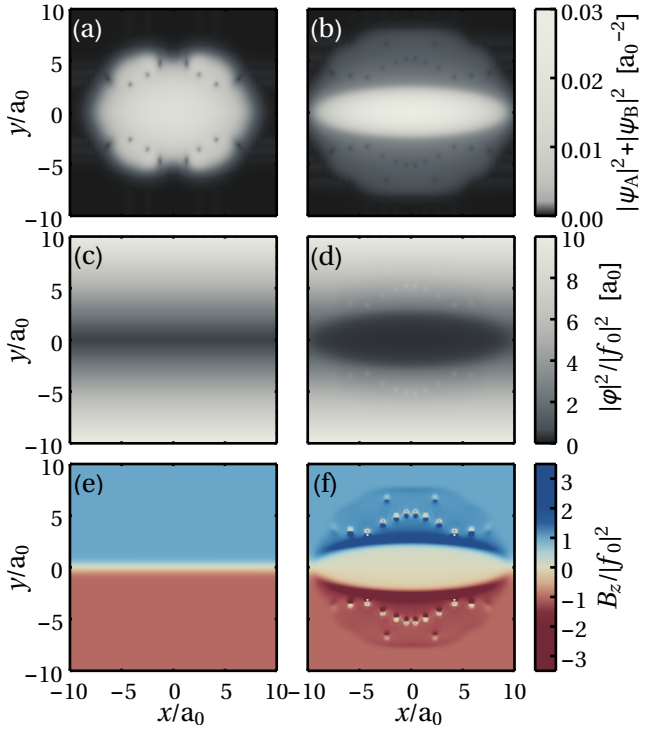

FIG. 2. (a) Ground state of condensate in a static field $|\varphi|^2 \propto |y|$ showing vortex formation. (b) Density of condensate when the field is allowed to evolve. No vortices remain in the cloud. (c) Relative intensity (i.e., $|\varphi|^2/|f_0|^2$) of light in cavity with no atom-light coupling used to generate (a). (d) Steady-state relative intensity of light when coupled to atomic cloud, showing reduction in region where atoms are present. Vortices remain in region of low atomic density where the intensity recovers and so the magnetic field is high. (e) Applied magnetic field (derivative of intensity in (c)) and (f) magnetic field after coupled evolution showing the applied field has been expelled from the condensate. All lengths are in units of the harmonic oscillator length $a_0 = 1/\sqrt{m\omega_x}$. Using ω_x as the frequency unit, other parameters are given by $\delta = -10$, $l = 1$, $\Delta_0 = -50$, $\kappa = 1000$, $\mathcal{E}_\Delta = 50$, $q = 70$, $\Omega = 10^5$, $mU = 1.5 \times 10^{-3}$, $N = 10^6$, and $f_0 = 4$, all relevant for cavity considered in [53, 54].

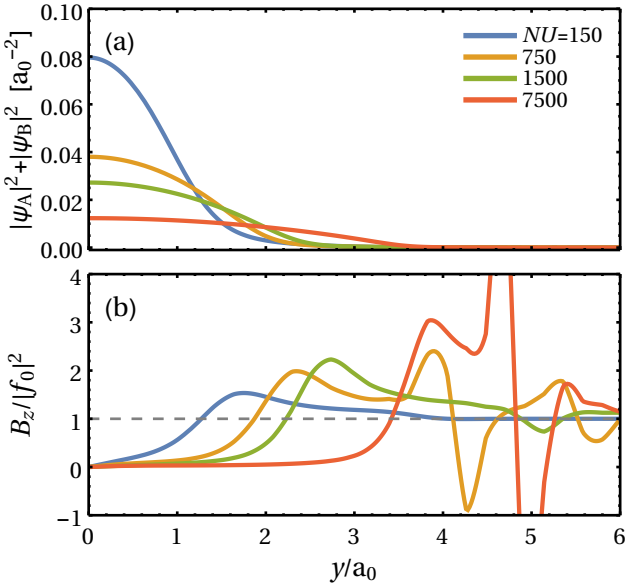

FIG. 3. Profile of (a) atomic density and (b) artificial field with varying number of atoms, in terms of the dimensionless parameter mNU. For realistic values, this corresponds to $N = 10^5$ (blue), $N = 5 \times 10^5$ (yellow), $N = 10^6$ (green), $N = 5 \times 10^6$ (orange). All other parameters are the same as in Fig. 2.

This diamagnetic response is shown in Fig. 2. Here we consider a source term $f(\mathbf{r})$, the pump field, which, in the absence of atoms, we set to have an intensity profile such that $|\varphi|^2 \propto |y|$, and thus the magnetic field has uniform magnitude, but with a sign dependent on y (see supplemental material [75]). The applied effective magnetic field is $B_z = \partial_y |\varphi|^2 \approx \pm |f_0|^2$, where f_0 is a constant which specifies the overall amplitude of the pump. The rows of Fig. 2 show the atomic density, the cavity intensity and the artificial magnetic field, respectively. The left column shows the case where the field is artificially kept static, i.e., where the terms proportional to $\psi_{A,B}$ are omitted from Eq. (2) to prevent any feedback, and the right column shows the case when the field is allowed to evolve.

As expected, in Fig. 2(f) we see that with the feedback included, the magnetic field is suppressed in the region containing the atomic cloud. Compared to the applied field (e), the field is suppressed in a large area where the atomic density, shown in (a), is high. This is a consequence of the change in cavity field which goes from being linear in $|y|$ as shown in (c), to having a region of near constant value shown in (d). This change in the intensity profile can be measured directly, and so the expulsion of the effective field can be reconstructed from the light emitted from the cavity. Additionally, as the cavity light intensity recovers to its default value, this causes an increase in its gradient, and so in panel (f) one sees the artificial magnetic field is increased immediately outside the atom cloud. In response to the changing field, we see that while in panel (a) there are vortices due to the static field, in panel (b) the higher density region no longer contains vortices, although they remain around the edges of the condensate where there is still high magnetic field. As in the case of the standard Abrikosov vortex lattice, the density of vortices depends on the local field strength, and the spacing goes from being larger than the size of the cloud to much smaller as the field recovers to its default value. This reduction in field $|\varphi|$ also leads to a change in the geometric scalar potential terms in Eq. (4), which is

what causes the condensate to shrink in size (see also below). Further out, the condensate density decays slowly in $\hat{y}$, and the remaining vortices lead to small modulations in the intensity. However, these modulations over small areas lead to quite large derivatives which show up as flux-antiflux pairs.

While the results in Fig. 2 clearly show suppression of the magnetic field analogous to the Meissner effect, it is important to note several differences between Eqs. (2) and (3) and the standard Meissner effect. In particular, while the atoms see an effective vector potential $|\varphi|^2\hat{\mathbf{x}}$, the remaining action for the field $|\varphi|^2$ does not simulate the Maxwell action for a gauge field: the remaining action does not have gauge symmetry, and has a small residual gap (due to the cavity loss and detuning). Because the action for φ is not gapless, there is already exponential decay of the synthetic field away from its source. What our results show is that coupling to a superfluid significantly enhances the gap for this field (in our case, by at least one order of magnitude), thus leading to a significant suppression of the field in the region where the atoms live. These differences mean that the distinction between type I and type II superconductivity is not clear. These points are discussed further in [75]. The effect of increasing the effective magnetic field strength is shown in the figure.

The figures are the result of numerical simulations of Eqs. (2) and (3) performed by using XMDS2 (eXtensible Multi-Dimensional Simulator) [77]. They represent the steady-state which is reached when the artificial magnetic field, proportional to the pump amplitude, is adiabatically increased from zero. A computationally efficient way to find this is to evolve the equation of motion for the light field, which includes pumping and loss, in real time, while simultaneously evolving the equation of motion for the condensate in imaginary time and renormalizing this wavefunction at each step. Hence, we find a state which is both a steady-state of the real-time equations of motion and also the ground state for the atoms in that given intensity profile. This method correctly finds the steady-state profile, but the transient dynamics does not match that which would be seen experimentally; as we focus only here on the steady-states. See supplementary video and [75] for real time evolution. We make use of the natural units of length and frequency set by the harmonic trap, i.e., $a_0 = 1/\sqrt{m\omega_x}$ and ω_x. For realistic experimental parameters, ω_x may be on the order of 1 kHz and $a_0 \approx 1\ \mu$m. Values of all other parameters are given in the figure captions.

The change in shape of the condensate in Fig. 2(c) can be explained by our choice of potential $V_{\rm ext}(\mathbf{r})$. As is clear from Eq. (4), the field φ leads both to vector and scalar potential terms. The scalar potentials have two contributions: quadratic and quartic. Analogous to the centrifugal force on a rotating condensate, these terms lead to a reduction (or even reversal) of the transverse harmonic trapping of the atoms. As a consequence of working at the tune-out wavelength, the quadratic scalar potentials in Eq. (4) are zero, i.e., $\mathcal{E}_\Sigma = 0$. The quartic term is harder to eliminate, but its effects can be compensated by choosing a trap of the form

$$V_{\rm ext} = \frac{m\omega_x^2}{2}\left(x^2+y^2\right) + \mathcal{E}_4|f_0|^4 y^2, \tag{6}$$

i.e., an asymmetric harmonic oscillator potential with $\omega_y = \sqrt{\omega_x^2 + 2\mathcal{E}_4|f_0|^2/m}$. However, this expression assumes $|\varphi|^2 = |f_0|^2|y|$, as would hold in the absence of atomic diamagnetism. As the magnetic field is expelled, the scalar potential also changes, and the condensate becomes more tightly trapped.

Figure 3 shows cross-sections at $x = 0$ of (a) the atomic density and (b) the artificial magnetic field for various values of the total number of atoms. Increasing the number of atoms leads to a larger condensate with a lower peak density (integral of density remains normalized). The resulting magnetic field profile is shown in (b). The area of low magnetic field is closely aligned to the area of high atomic density. At the edges of the cloud, the artificial field is increased as the expelled field accumulates here, before returning to its default value well outside the cloud. The effect of vortices in the very low density areas can also be seen. Varying other parameters leads to similar physics, which can be understood in terms of the effective parameters introduced in Eq. (4). The effect of varying the effective field strength is discussed further in [75].

In summary, we have shown how a spatially varying synthetic gauge field can be achieved, and how magnetic field suppression in an atomic superfluid, analogous to the Meissner effect, can be realized. By effecting an artificial magnetic field proportional to the intensity of light in a multimode cavity, we have coupled the dynamics of the spatial profile of the magnetic field and the atomic wavefunction. Our results illustrate the potential of multimode cavity QED to simulate dynamical gauge fields, and to explore self-consistent steady states, and potentially phase transitions, of matter coupled to synthetic gauge fields.

We acknowledge helpful discussions with E. Altman, M. J. Bhaseen, S. Gopalakrishnan, B. D. Simons, and I. Spielman. We thank V. D. Vaidya and Y. Guo for help in preparation of the manuscript. K.E.B. and J.K. acknowledge support from EPSRC program TOPNES (EP/I031014/1). J.K. acknowledges support from the Leverhulme Trust (IAF-2014-025). B.L.L. acknowledges support from the ARO and the David and Lucille Packard Foundation.

[1] W. Meissner and R. Ochsenfeld, Naturwissenschaften **21**, 787 (1933).

[2] A. Leggett, *Quantum Liquids: Bose Condensation and Cooper Pairing in Condensed-matter Systems*, Oxford graduate texts in mathematics (OUP Oxford, 2006).

[3] V. L. Ginzburg and L. D. Landau, Zh. Eksp. Teor. Fiz **20**, 1064 (1950).

[4] J. R. Schrieffer, *Theory of Superconductivity* (Westview Press, Boulder, CO, 1983).

[5] F. London and H. London, Proc. R. Soc. A **149**, 71 (1935).

[6] P. W. Anderson, Phys. Rev. **130**, 439 (1963).

[7] P. W. Higgs, Phys. Rev. Lett. **13**, 508 (1964).

[8] P. M. Visser and G. Nienhuis, Phys. Rev. A **57**, 4581 (1998).

[9] G. Juzeliūnas and P. Öhberg, Phys. Rev. Lett. **93**, 033602 (2004).

[10] I. B. Spielman, Phys. Rev. A **79**, 063613 (2009).

[11] Y.-J. Lin, R. L. Compton, A. R. Perry, W. D. Phillips, J. V. Porto, and I. B. Spielman, Phys. Rev. Lett. **102**, 130401 (2009).

[12] Y.-J. Lin, R. L. Compton, K. Jimenez-Garcia, J. V. Porto, and I. B. Spielman, Nature (London) **462**, 628 (2009).

[13] D. Jaksch and P. Zoller, New J. Phys. **5**, 56 (2003).

[14] A. S. Sørensen, E. Demler, and M. D. Lukin, Phys. Rev. Lett. **94**, 086803 (2005).

[15] A. R. Kolovsky, Europhys. Lett. **93**, 20003 (2011).

[16] N. R. Cooper, Phys. Rev. Lett. **106**, 175301 (2011).

[17] J. Struck, C. Ölschläger, R. Le Targat, P. Soltan-Panahi, A. Eckardt, M. Lewenstein, P. Windpassinger, and K. Sengstock, Science **333**, 996 (2011).

[18] M. Aidelsburger, M. Atala, S. Nascimbène, S. Trotzky, Y.-A. Chen, and I. Bloch, Phys. Rev. Lett. **107**, 255301 (2011).

[19] P. Hauke, O. Tieleman, A. Celi, C. Ölschläger, J. Simonet, J. Struck, M. Weinberg, P. Windpassinger, K. Sengstock, M. Lewenstein, and A. Eckardt, Phys. Rev. Lett. **109**, 145301 (2012).

[20] J. Struck, C. Ölschläger, M. Weinberg, P. Hauke, J. Simonet, A. Eckardt, M. Lewenstein, K. Sengstock, and P. Windpassinger, Phys. Rev. Lett. **108**, 225304 (2012).

[21] H. Miyake, G. A. Siviloglou, C. J. Kennedy, W. C. Burton, and W. Ketterle, Phys. Rev. Lett. **111**, 185302 (2013).

[22] M. Aidelsburger, M. Atala, M. Lohse, J. T. Barreiro, B. Paredes, and I. Bloch, Phys. Rev. Lett. **111**, 185301 (2013).

[23] M. Atala, M. Aidelsburger, M. Lohse, J. T. Barreiro, B. Paredes, and I. Bloch, Nat. Phys. **10**, 588 (2014).

[24] J. Dalibard, F. Gerbier, G. Juzeliūnas, and P. Öhberg, Rev. Mod. Phys. **83**, 1523 (2011).

[25] N. Goldman, G. Juzeliūnas, P. Öhberg, and I. B. Spielman, Rep. Prog. Phys. **77**, 126401 (2014).

[26] H. Zhai, Int. J. Mod. Phys. B **26**, 1230001 (2012).

[27] H. Zhai, Rep. Prog. Phys. **78**, 026001 (2015).

[28] N. Schine, A. Ryou, A. Gromov, A. Sommer, and J. Simon, Nature (London) **534**, 671 (2016).

[29] K. Fang, Z. Yu, and S. Fan, Nat. Photon. **6**, 782 (2012).

[30] M. Hafezi, S. Mittal, J. Fan, A. Migdall, and J. M. Taylor, Nat. Photon. **7**, 1001 (2013).

[31] T. Dubček, K. Lelas, D. Jukić, R. Pezer, M. Soljačić, and H. Buljan, New J. Phys. **17**, 125002 (2015).

[32] G. B. Hess and W. M. Fairbank, Phys. Rev. Lett. **19**, 216 (1967).

[33] S. Walter and F. Marquardt, "Dynamical Gauge Fields in Optomechanics," (2015), arXiv:1510.06754.

[34] W. Zheng and N. R. Cooper, "Superradiance induced particle flow via dynamical gauge coupling," (2016), arXiv:1604.06630.

[35] P. Domokos and H. Ritsch, Phys. Rev. Lett. **89**, 253003 (2002).

[36] A. T. Black, H. W. Chan, and V. Vuletić, Phys. Rev. Lett. **91**, 203001 (2003).

[37] K. Baumann, C. Guerlin, F. Brennecke, and T. Esslinger, Nature (London) **464**, 1301 (2010).

[38] Y. Deng, J. Cheng, H. Jing, and S. Yi, Phys. Rev. Lett. **112**, 143007 (2014).

[39] L. Dong, L. Zhou, B. Wu, B. Ramachandhran, and H. Pu, Phys. Rev. A **89**, 011602 (2014).

[40] B. Padhi and S. Ghosh, Phys. Rev. A **90**, 023627 (2014).

[41] J.-S. Pan, X.-J. Liu, W. Zhang, W. Yi, and G.-C. Guo, Phys. Rev. Lett. **115**, 045303 (2015).

[42] L. Dong, C. Zhu, and H. Pu, Atoms **3**, 182 (2015).

[43] C. Kollath, A. Sheikhan, S. Wolff, and F. Brennecke, Phys. Rev. Lett. **116**, 060401 (2016).

[44] A. Sheikhan, F. Brennecke, and C. Kollath, Phys. Rev. A **93**, 043609 (2016).

[45] S. Gopalakrishnan, B. L. Lev, and P. M. Goldbart, Nat. Phys. **5**, 845 (2009).

[46] H. Talbot, Philos. Mag. Series 3 **9**, 401 (1836).

[47] T. Ackemann and W. Lange, Appl. Phys. B **72**, 21 (2001).

[48] G. Labeyrie, E. Tesio, P. M. Gomes, G.-L. Oppo, W. J. Firth, G. R. M. Robb, A. S. Arnold, R. Kaiser, and T. Ackemann, Nat. Photon. **8**, 321 (2014).

[49] M. Diver, G. R. M. Robb, and G.-L. Oppo, Phys. Rev. A **89**, 033602 (2014).

[50] G. R. M. Robb, E. Tesio, G.-L. Oppo, W. J. Firth, T. Ackemann, and R. Bonifacio, Phys. Rev. Lett. **114**, 173903 (2015).

[51] S. Gopalakrishnan, B. Lev, and P. Goldbart, Phys. Rev. A **82**, 34 (2010).

[52] A. Wickenbrock, M. Hemmerling, G. R. M. Robb, C. Emary, and F. Renzoni, Phys. Rev. A **87**, 043817 (2013).

[53] A. J. Kollár, A. T. Papageorge, K. Baumann, M. A. Armen, and B. L. Lev, New J. Phys. **17**, 043012 (2015).

[54] A. J. Kollár, A. T. Papageorge, V. D. Vaidya, Y. Guo, J. Keeling, and B. L. Lev, "Supermode-Density-Wave-Polariton Condensation," (2016), arXiv:1606.04127.

[55] S. Tewari, V. W. Scarola, T. Senthil, and S. D. Sarma, Phys. Rev. Lett. **97**, 200401 (2006).

[56] J. I. Cirac, P. Maraner, and J. K. Pachos, Phys. Rev. Lett. **105**, 190403 (2010).

[57] E. Zohar and B. Reznik, Phys. Rev. Lett. **107**, 275301 (2011).

[58] E. Zohar, J. I. Cirac, and B. Reznik, Phys. Rev. Lett. **109**, 125302 (2012).

[59] D. Banerjee, M. Dalmonte, M. Müller, E. Rico, P. Stebler, U.-J. Wiese, and P. Zoller, Phys. Rev. Lett. **109**, 175302 (2012).

[60] D. Banerjee, M. Bögli, M. Dalmonte, E. Rico, P. Stebler, U.-J. Wiese, and P. Zoller, Phys. Rev. Lett. **110**, 125303 (2013).

[61] M. J. Edmonds, M. Valiente, G. Juzeliūnas, L. Santos, and P. Öhberg, Phys. Rev. Lett. **110**, 085301 (2013).

[62] E. Zohar, J. I. Cirac, and B. Reznik, Phys. Rev. A **88**,

023617 (2013).
[63] E. Zohar, J. I. Cirac, and B. Reznik, Phys. Rev. Lett. **110**, 055302 (2013).
[64] K. Kasamatsu, I. Ichinose, and T. Matsui, Phys. Rev. Lett. **111**, 115303 (2013).
[65] E. Zohar, J. I. Cirac, and B. Reznik, Rep. Prog. Phys. **79**, 014401 (2016).
[66] P. Hauke, D. Marcos, M. Dalmonte, and P. Zoller, Phys. Rev. X **3**, 041018 (2013).
[67] L. Tagliacozzo, A. Celi, A. Zamora, and M. Lewenstein, Ann. Phys. (N. Y.) **330**, 160 (2013).
[68] D. Yang, G. Shankar Giri, M. Johanning, C. Wunderlich, P. Zoller, and P. Hauke, "Analog Quantum Simulation of (1+1)D Lattice QED with Trapped Ions," (2016), arXiv:1604.03124.
[69] E. A. Martinez, C. A. Muschik, P. Schindler, D. Nigg, A. Erhard, M. Heyl, P. Hauke, M. Dalmonte, T. Monz, P. Zoller, and R. Blatt, Nature (London) **534**, 516 (2016).
[70] D. Marcos, P. Rabl, E. Rico, and P. Zoller, Phys. Rev. Lett. **111**, 110504 (2013).
[71] D. Marcos, P. Widmer, E. Rico, M. Hafezi, P. Rabl, U.-J. Wiese, and P. Zoller, Ann. Phys. (N. Y.) **351**, 634 (2014).
[72] A. T. Papageorge, A. J. Kollár, and B. L. Lev, Opt. Express **24**, 11447 (2016).
[73] L. J. LeBlanc, M. C. Beeler, K. Jiménez-García, R. A. Williams, W. D. Phillips, and I. B. Spielman, New J. Phys. **17**, 065016 (2015).
[74] F. Schmidt, D. Mayer, M. Hohmann, T. Lausch, F. Kindermann, and A. Widera, Phys. Rev. A **93**, 022507 (2016).
[75] Supplemental material, containing details of reduction to effective 2D equations, details of numerical simulation, discussion of artificial magnetic field strength suppression in the geometry under consideration, and evolution in real time.
[76] A. E. Siegman, *Lasers* (University Science Books, Sausolito, 1986).
[77] G. R. Dennis, J. J. Hope, and M. T. Johnsson, Comput. Phys. Commun. **184**, 201 (2013).

Supplemental Materials: Meissner-like effect for synthetic gauge field in multimode cavity QED

Kyle E. Ballantine,[1] Benjamin L. Lev,[2] and Jonathan Keeling[1]

[1] *SUPA, School of Physics and Astronomy, University of St. Andrews, St. Andrews KY16 9SS, United Kingdom*

[2] *Departments of Physics and Applied Physics and Ginzton Laboratory, Stanford University, Stanford CA 94305, USA*

In this supplemental material, we discuss the reduction from the full three-dimensional problem of atoms in an anisotropic trap coupled to cavity modes, to the effective two-dimensional equations for atoms and cavities. We also present further details and results of the numerical simulations, and discuss further the nature of the magnetic field suppression in the two-dimensional geometry we consider, and the corresponding surface current profiles.

REDUCTION TO EFFECTIVE TWO-DIMENSIONAL EQUATIONS

To derive the equations of motion Eqs. (2) and (3), we need to use the structure of the cavity modes to eliminate the z dependence. The intensity of light in the cavity can be expressed as a sum of cavity eigenmodes u_μ,

$$\hat{I}(\mathbf{r}) = \left|\sum \hat{a}_\mu u_\mu(\mathbf{r},z)\right|^2, \tag{1}$$

where the mode functions take the form

$$u_\mu(\mathbf{r},z) = \chi_\mu(\mathbf{r})\cos(g(z)+\theta(z)(\mu_x+\mu_y)). \tag{2}$$

Here χ_μ are normalized Hermite-Gauss modes with index $\mu_{x(y)}$ in the $x(y)$ directions respectively, i.e., $\chi_\mu(\mathbf{r}) = \chi_{\mu_x}(\sqrt{2}x/w)\chi_{\mu_y}(\sqrt{2}y/w)/w$ with

$$\chi_{\mu_x}(\tilde{x}) = \sqrt[4]{\frac{2}{\pi}}\frac{1}{\sqrt{2^{\mu_x}\mu_x!}}H_{\mu_x}(\tilde{x})e^{-\tilde{x}^2}, \tag{3}$$

and similarly for y, where $w = w_0\sqrt{1+(z/z_R)^2}$ is the beam waist and H_n is the nth Hermite function. $g(z) = k[z+r^2/2R(z)]-\Phi(z)$ in terms of the Gouy phase $\Phi(z) = \arctan(z/z_R)$ [1], the radius of curvature is $R(z) = z + z_R^2/z$, and $\theta(z) = \Phi(z)+\pi/4$. Here z_R is the Rayleigh range, $z_R = kw_0^2/2$. The mode amplitudes $\alpha_\mu = \langle\hat{a}_\mu\rangle$ follow the equation of motion $i\partial_t\alpha_\mu = \left\langle\left[\hat{a}_\mu,\hat{H}\right]\right\rangle - i\kappa\alpha_\mu$, where $\hat{H} = \hat{H}_{\rm atom}+\hat{H}_{\rm cav}+f_\mu(\hat{a}_\mu^\dagger+\hat{a}_\mu)$ and f_μ is the overlap of the pump beam with each mode. This gives

$$\begin{aligned} i\partial_t\alpha_\mu &= (\omega_\mu-\omega_P-i\kappa)\alpha_\mu + f_\mu - P_{\mu\nu}\alpha_\nu \\ P_{\mu\nu} &= \frac{1}{2}\int \mathrm{d}^2\mathbf{r}\,\mathrm{d}z\, u_\mu u_\nu(\mathcal{E}_A|\Psi_A|^2+\mathcal{E}_B|\Psi_B|^2), \end{aligned} \tag{4}$$

where ω_μ is the frequency of mode μ.

As discussed in the main text, we consider a pancake of atoms by writing $\Psi_{A,B}(\mathbf{r},z) = \psi_{A,B}(\mathbf{r})Z(z)$ where

$$|Z(z)|^2 = \frac{1}{\sqrt{2\pi\sigma_z^2}}\exp\left(-\frac{(z-z_0)^2}{2\sigma_z^2}\right). \tag{5}$$

We can then eliminate the z dependence from all the above terms, and write effective transverse dynamics of atoms and light. To proceed, we compute the integral

$$I_\perp(\mathbf{r}) = \int \mathrm{d}z\,|Z(z)|^2 I(\mathbf{r},z). \tag{6}$$

To do this, we work in the approximation that $\lambda \ll \sigma_z \ll z_R$ so that we can drop the fast oscillating terms depending on $g(z)$ and evaluate $\theta(z)$ at $z = z_0$. This gives

$$\begin{aligned} &\int \mathrm{d}z\,|Z(z)|^2 u_\mu(\mathbf{r},z)u_\nu(\mathbf{r},z) \approx \\ &\qquad \frac{1}{2}\chi_\mu(\mathbf{r})\chi_\nu(\mathbf{r})\cos(\theta(z_0)(\mu_x+\mu_y-\nu_x-\nu_y)). \end{aligned} \tag{7}$$

This allows us to write the dynamics of $\psi_{A,B}(\mathbf{r})$ in terms of the cavity mode amplitudes α_μ.

Turning to the equations for the cavity mode amplitudes, we first define the transverse field as

$$\varphi(\mathbf{r}) = \sum \alpha_\mu\chi_\mu(\mathbf{r}). \tag{8}$$

With this definition, we multiply Eq. (4) by $\chi_\mu(\mathbf{r}')$ and sum over μ to get the equation of motion for $\varphi(\mathbf{r}')$. In order to be able to write the transverse dynamics of the light field in real space, we use the fact that Hermite-Gauss modes are eigenmodes of the harmonic oscillator Hamiltonian

$$\omega_\mu\chi_\mu(\mathbf{r}) = \left[\frac{\delta}{2}\left(-l^2\nabla^2+\frac{r^2}{l^2}\right)+\omega_0\right]\chi_\mu(\mathbf{r}), \tag{9}$$

where the beam waist is $\sqrt{2}l$, ω_0 is the frequency of the confocal cavity, and δ is the mode spacing when the cavity is not perfectly confocal.

To close the equations, we must write $I_\perp(\mathbf{r})$ in terms of $\varphi(\mathbf{r})$. For a general z_0, the light in the cavity will mediate non-local interactions between the atoms, and so this involves a convolution. However, we will assume that the atoms are close to the end of the cavity, which in the confocal case is at $z_0 = -z_R$. This leads to a quasi-local matter-light interaction, and thus, as we see in the main text, provides a close analog to the standard

Meissner effect. Since $\theta(-z_R) = 0$, the cosine term drops out of Eq. (7), and so $I_\perp(\mathbf{r}) = |\varphi(\mathbf{r})|^2/2$. Together with the relation

$$\sum \chi_\mu(\mathbf{r})\chi_\mu(\mathbf{r}') = \delta(\mathbf{r}-\mathbf{r}'), \tag{10}$$

this leads to the equation of motion for the 2D cavity field, which combined with the equation of motion of the atom condensate, describes the dynamics of the system. As can be seen from Eq. 7, a small non-zero Gouy phase can be neglected for low-order Hermite-Gauss modes, but will become more relevant for higher-order modes. To describe the dynamics at small length scales requires these high-order-modes and so would require the calculation of non-local correlations. However since the intensity is relatively smooth, the profile can be captured well with a reasonable number of modes. Using up to $\mu_y = 26$ gives excellent agreement, reproducing the field amplitude with an error $< 5\%$. For this set of modes, the cosine term is always > 0.86 if the center of the cloud is trapped 200 μm or less from the mirror.

FURTHER DETAILS OF NUMERICAL SIMULATION

In order to have an approximately constant artificial magnetic field over a large area while keeping the intensity symmetric, we choose a pump profile

$$f(\mathbf{r}) = f_0\sqrt{|y|}\sqrt{\kappa^2 + (\delta r^2/2l^2 - \Delta_0)^2} \tag{11}$$

which, in an empty cavity, would give $|\varphi|^2 \approx |f_0|^2|y|$. We then convolve this profile with a Gaussian of width 0.5 so that it is smoothed near $y = 0$. Hence $B_z \approx \pm|f_0|^2$, as shown in Fig. [2](c). Such a profile can be achieved using, e.g., a digital multimirror device (DMD) [2].

NATURE OF SUPPRESSION OF MAGNETIC FIELD INSIDE ATOM CLOUD

Distinctions from Ginzburg-Landau equations

As noted in the main text, there are some distinctions between the behavior we predict here, and the standard Meissner effect. This section discusses in further detail the origin of these distinctions.

In the standard Meissner effect, there is a vector potential A_μ which couples (via minimal coupling) to the matter component. The remaining action for the system then takes the Maxwell form, $F_{\mu\nu}F^{\mu\nu}$, in terms of the field tensor $F_{\mu\nu} = \partial_\mu A_\nu - \partial_\nu A_\mu$. Our equations of motion correspond to an action that differs in several ways. Firstly, our action is non-relativistic (i.e., not Lorenz covariant): this affects the dynamics, but not the steady state. Secondly, our action is not gauge invariant—i.e., our action depends directly on $|\varphi|^2$, which plays the role of the vector potential, rather than depending only on derivatives of this quantity. Thirdly, while the quantity $|\varphi|^2\hat{\mathbf{x}}$ plays the role of the vector potential $\mathbf{A}$ in terms of minimal coupling, the "free action" has the terms of the form $(\nabla\varphi)^2$, which is quite different (in terms of powers of φ) to the Maxwell action noted above. Finally, and most importantly of these differences, our action is not gapless. This last difference, which occurs due to the inevitable cavity loss terms, means that there is no sharp distinction between the case of coupling to superfluid or normal atoms: the magnetic field always has a finite penetration depth—i.e., away from the location of the source term $f(\mathbf{r})$, the field φ will decay. However, in our numerical results, we clearly see a dramatic change in the suppression of the magnetic field. This is consistent, as the effect we are seeing can be understood as arising from a dramatic enhancement of the effective gap. Explicitly, in Eq. (2), the superfluid induced gap, $N\mathcal{E}_\Delta(|\psi_A|^2 - |\psi_B|^2)$, is at least an order of magnitude larger than the other terms κ and Δ_0, leading to a large suppression of the magnetic field. However, this suppression does not lead to the simple analogue of the London equation $\nabla^2\mathbf{A} = -\mathbf{A}/\lambda^2$, and thus there is no simple definition of effective penetration depth. This is because of the differences noted above, that the minimal coupling term has $|\varphi|^2\hat{\mathbf{x}}$ play the role of $\mathbf{A}$ (which determines the right hand side of the London equation), but the free action involves $(\nabla\varphi)^2$, which determines the left hand side. The differing powers of φ in these lead to a non-linear London equation, without a simple length scale.

An additional difference from textbook Meissner physics arises because of the distinct geometry of our system. In our geometry, both the atom cloud, and the synthetic field vary only in the transverse two-dimensional plane. In the textbook example of the Meissner example, a piece of superconducting material is placed in an externally imposed uniform magnetic field. However, imposing an uniform field requires sources, e.g., loops of free current placed far away in the z direction. In our geometry, with the synthetic field restricted to two dimensions, this is not possible. The source of the vector potential (in our case the longitudinal pumping term, $f(\mathbf{r})$), must live in the same plane as the material. Generating a pseudo uniform magnetic field thus requires an extended source term. The specific case we consider has this source exist across the entire plane. Thus, we cannot expect complete expulsion of the magnetic field, but only suppression. This, combined with the above issues in defining an effective penetration length, mean it is not straightforward to distinguish type I and type II behavior in this geometry. Nevertheless, as discussed below, one can explore quantitatively how behavior varies with increasing field strength.

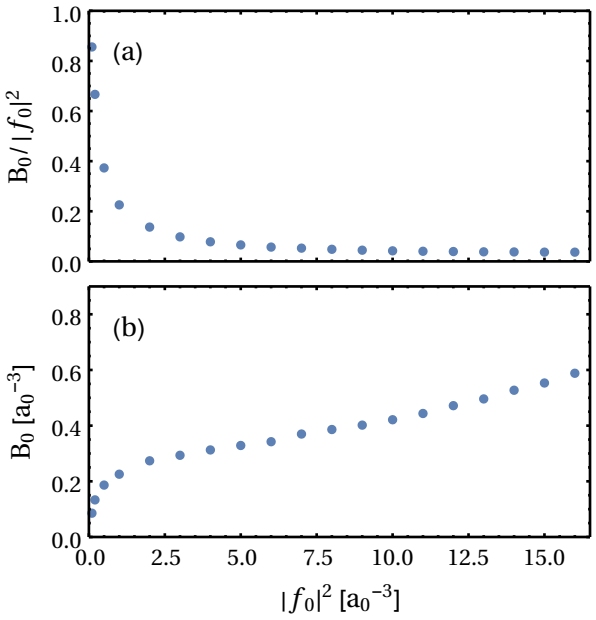

FIG. 1. Plateau value of magnetic field inside condensate (a) normalized by pump intensity and (b) unnormalized as a function of pump intensity. Increasing pump strength leads to a stronger diamagnetic response so that the relative field falls and the absolute value of the field increases sub linearly for small pump intensities. We choose $NU = 7500$ and all other parameters are the same as Fig. [2].

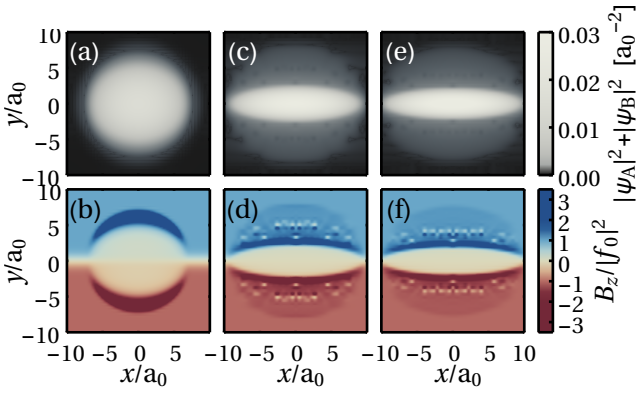

FIG. 2. The atomic density (top row) and relative effective magnetic field (bottom row) is plotted for a variety of field strengths; (a) and (b) $|f_0|^2 = 6$, (c) and (d) $|f_0|^2 = 19$, and (e) and (f) $|f_0|^2 = 22$. As the pump strength increases, the cloud becomes more tightly trapped in the y direction. The effective field in the middle of the cloud also becomes more suppressed relative to the pump strength. All parameters in these plots are the same as in Fig. 2.

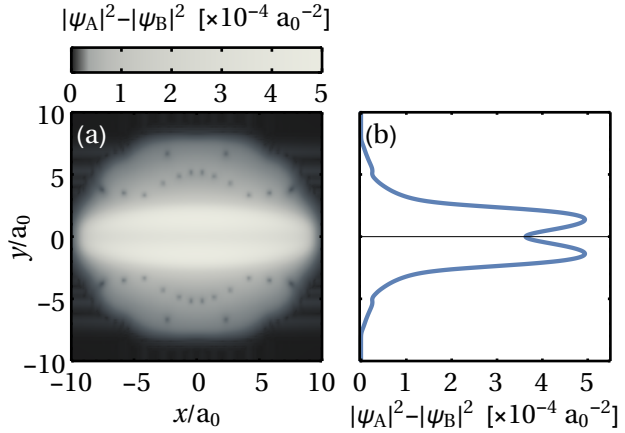

FIG. 3. (a) $|\psi_A|^2 - |\psi_B|^2$ and (b) a cross-section of this quantity at $x = 0$. This term, through which the atomic motion feeds back into the evolution of the light field, is relatively large at the edge of the cloud analogous to supercurrents at the surface of a superconductor.

Evolution of spatial profile with increasing field

To explore the above issues further numerically, Fig. S1 shows the artificial magnetic field inside the condensate (at $x = 0$, $y/a_0 = 1$) as a function of pump intensity (or equivalently, applied field strength). Most terms in Eq. (2) are linear in φ. However the diamagnetic response, according to Eq. (5), is proportional to $|\varphi|^2$. Hence, for very low pump strength it is approximately zero and the resulting field is equal to the applied field. As the pump intensity increases, the diamagnetic term begins to dominate. One thus observes that the relative field strength falls by several orders of magnitude. Equivalently, the absolute field strength increases sublinearly. The mean-field approximation cannot describe the ultimate breakdown of superfluidity. Thus, within this approximation, as long as the scalar potential terms are properly compensated so that the cloud retains a finite width, the relative field strength continues to fall. Beyond mean field theory, quantum and thermal fluctuations may destroy the superfluidity. The details of how this happens are an interesting question for future work. The atomic density and effective magnetic field profiles are shown in Fig. 2 for low, medium and high pump strength.

Role of surface currents

Figure 3 shows the quantity $|\psi_A|^2-|\psi_B|^2$. As discussed in the main text, this quantity appears in the equation of motion for φ, and acts to suppress the cavity light field dependent on the state of the atoms. As also observed from Eq.(5), this quantity is proportional to the x

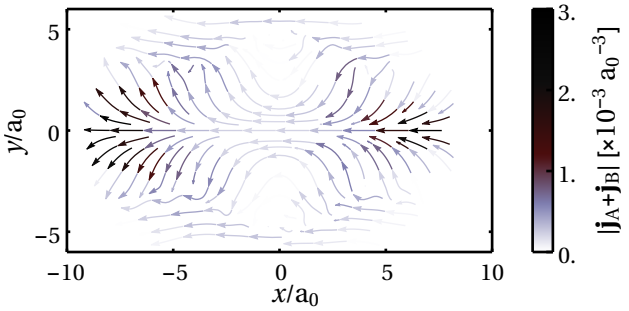

FIG. 4. Total current $(\psi_A, \psi_B)^* \cdot \nabla(\psi_A, \psi_B)^T - \text{c.c} = \mathbf{j}_A + \mathbf{j}_B$. This is shown as a stream plot of continuous streamlines following the local direction, with the magnitude represented by the color of the lines.

component of the current. One can see that this term is peaked near the edge of the region from which the field is expelled, so, analogous to the standard Meissner effect, the x component of the current describes how surface currents suppress the field inside the condensate.

The full current $(\psi_A, \psi_B)^* \cdot \nabla(\psi_A, \psi_B)^T - \text{c.c}$ can also be evaluated. This total kinetic current in plotted in Fig. 4. Note that, when considering the original fields ψ_A, ψ_B, the current is the typical kinetic current as there is no vector potential acting on these components. Since this current is not what appears as a source term in the light equation of motion we do not expect it to be related in a simple way to the resulting effective magnetic field.

REAL-TIME DYNAMICS

To support the ground state calculations in the main text, we have also calculated the evolution of the system in real time. We start the evolution from the ground state of the harmonic trap, in the Raman beams, as the pump strength is adiabatically increased from 0 to the final value. We choose a linear pump ramp with a total time of $50/\omega_x \lesssim 100$ms.

A supplemental video, showing the time evolution of the synthetic magnetic field is provided. The final state found from this simulation is shown in Fig. 5, compared against the ground state. Because the real time evolution is computationally costly, it is necessary to use a much lower spatial resolution than used for the exact ground state, thus these results are more strongly affected by numerical noise. However the main features of the actual ground state, namely a region of excluded magnetic field, surrounded by a region of high field which then returns to the default value, are clear to see.

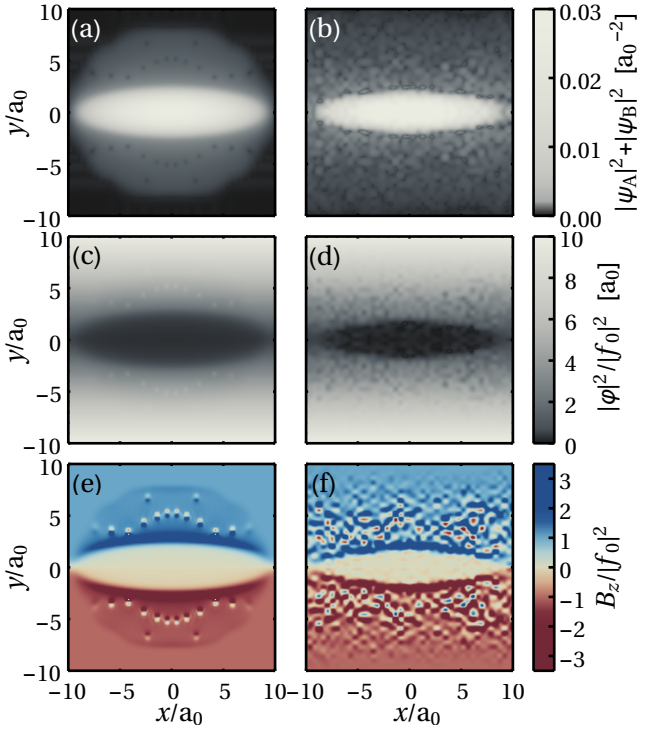

FIG. 5. Comparison of the exact ground state (left column) and the result of adiabatic evolution (right column) for the atomic density ((a), (b)), the intensity ((c), (d)) and the effective magnetic field ((e), (f)). All parameters are the same as Fig. [2]. The pump amplitude is linearly ramped over a timescale $50/\omega_x$. The real-time simulations suffer from excess noise due to the limited resolution, but (f) shows that the main features of the magnetic field in the ground state are preserved.

[1] A. E. Siegman, *Lasers* (University Science Books, Sausolito, 1986).

[2] A. T. Papageorge, A. J. Kollár, and B. L. Lev, Opt. Express **24**, 11447 (2016).